

Article

In Situ Fabrication of SnS₂/SnO₂ Heterostructures for Boosting Formaldehyde—Sensing Properties at Room Temperature

Dan Meng¹, Zongsheng Xie¹, Mingyue Wang², Juhua Xu³, Xiaoguang San^{1,*}, Jian Qi⁴, Yue Zhang¹, Guosheng Wang¹ and Quan Jin^{3,*}

¹ College of Chemical Engineering, Shenyang University of Chemical Technology, Shenyang 110142, China; mengdan0610@hotmail.com (D.M.); xzs19991015@163.com (Z.X.); meat_d@163.com (Y.Z.); m18240179987@163.com (G.W.)

² Institute for Superconducting and Electronic Materials (ISEM), Australian Institute for Innovative Materials (AIIM), Innovation Campus, University of Wollongong, Squires Way, North Wollongong, NSW 2500, Australia; mw663@uowmail.edu.au

³ Key Laboratory of Automobile Materials (Ministry of Education), School of Materials Science and Engineering, Jilin University, Changchun 130022, China; hmm9911057@163.com

⁴ State Key Laboratory of Biochemical Engineering, Institute of Process Engineering, Chinese Academy of Sciences, Beijing 100190, China; jq@ipe.ac.cn

* Correspondence: sanxiaoguang@syuct.edu.cn (X.S.); qjin@jlu.edu.cn (Q.J.)

Abstract: Formaldehyde, as a harmful gas produced by materials used for decorative purposes, has a serious impact on human health, and is also the focus and difficulty of indoor environmental pollution prevention; hence, designing and developing gas sensors for the selective measurement of formaldehyde at room temperature is an urgent task. Herein, a series of SnS₂/SnO₂ composites with hollow spherical structures were prepared by a facile hydrothermal approach for the purpose of formaldehyde sensing at room temperature. These novel hierarchical structured SnS₂/SnO₂ composites-based gas sensors demonstrate remarkable selectivity towards formaldehyde within the concentration range of sub-ppm (0.1 ppm) to ppm (10 ppm) at room temperature. Notably, the SnS₂/SnO₂-2 sensor exhibits an exceptional formaldehyde-sensing performance, featuring an ultra-high response (1.93, 0.1 ppm and 17.51, 10 ppm), as well as good repeatability, long-term stability, and an outstanding theoretical detection limit. The superior sensing capabilities of the SnS₂/SnO₂ composites can be attributed to multiple factors, including enhanced formaldehyde adsorption, larger specific surface area and porosity of the hollow structure, as well as the synergistic interfacial incorporation of the SnS₂/SnO₂ heterojunction. Overall, the excellent gas sensing performance of SnS₂/SnO₂ hollow spheres has opened up a new way for their detection of trace formaldehyde at room temperature.

Keywords: SnS₂/SnO₂; n-n heterostructures; formaldehyde sensing; room temperature; DFT calculations



Citation: Meng, D.; Xie, Z.; Wang, M.; Xu, J.; San, X.; Qi, J.; Zhang, Y.; Wang, G.; Jin, Q. In Situ Fabrication of SnS₂/SnO₂ Heterostructures for Boosting Formaldehyde—Sensing Properties at Room Temperature. *Nanomaterials* **2023**, *13*, 2493. <https://doi.org/10.3390/nano13172493>

Academic Editor: Lyubov G. Bulusheva

Received: 6 August 2023

Revised: 24 August 2023

Accepted: 1 September 2023

Published: 4 September 2023



Copyright: © 2023 by the authors. Licensee MDPI, Basel, Switzerland. This article is an open access article distributed under the terms and conditions of the Creative Commons Attribution (CC BY) license (<https://creativecommons.org/licenses/by/4.0/>).

1. Introduction

Formaldehyde in indoor environments mainly comes from plywood, density board, paint, etc., in decoration materials. Due to the large use of urea formaldehyde resin adhesive materials, formaldehyde pollution in indoor air is aggravated [1], which causes serious health concerns. Even low concentrations of formaldehyde can cause breathing difficulties and headaches in humans [2]. More importantly, high concentrations of formaldehyde can disrupt the central nervous system and immune system and cause respiratory diseases and blindness [3]. Notably, multiple medical organizations and institutions around the world have proposed that formaldehyde's maximum permissible occupational exposure concentration is 0.75 ppm over 8 h and 2 ppm over 15 min [4]; therefore, accurate detection of trace formaldehyde is highly desirable for human health.

Currently, many analytical technologies, e.g., electrochemistry [5], chromatography [6], fluorescence [7], and spectrophotometry [8], are available for detecting formaldehyde; however, they need to overcome the drawbacks of large equipment size and expensive and complicated operation, which limit their application in daily life. Under these circumstances, metal oxide semiconductors (MOS) have attracted great attention as gas sensors because of their simple operation, easy fabrication, and real-time monitoring [9,10], which have become a very effective means of formaldehyde gas detection. In the past five years, different types of MOS materials, such as ZnO [11], SnO₂ [12], NiO [13], In₂O₃ [14], and CuO [15], have been used to fabricate gas sensors and offer good sensitivity to formaldehyde. Among them, n-type tin dioxide (SnO₂) has attracted widespread attention for monitoring various reduced or oxide gases due to its excellent thermal stability [16], compatibility, and multiple morphologies [17,18]. Research has shown that SnO₂ could be a promising formaldehyde gas-sensing material. Nonetheless, the commonly used SnO₂ sensor shows low sensitivity and poor selectivity and usually works under high-power consumption limited to fulfilling the demands of integration and intelligence; therefore, room-temperature operating sensing materials with the capability to detect formaldehyde are being intensively explored to meet the requirement for portable or Internet of Things applications [19].

In recent years, many published studies have demonstrated that the three-dimensional (3D) hierarchical micro-nano structures of SnO₂ possess numerous active sites and abundant mesopores. These structural features facilitate rapid gas diffusion and adsorption of gas molecules on the surface, thereby imparting excellent gas sensing properties [20–22]; however, characterizing the gas-sensing capabilities of these structures at room temperature presents a significant challenge. Recently, researchers have made considerable efforts to address this issue by constructing heterostructures using one or more different materials. These heterojunctions have been shown to have a noticeable impact on adjusting the intrinsic electronic properties of SnO₂, thereby achieving an outstanding gas-sensing performance [23–26]. Particularly, tin disulfide (SnS₂), as a representative Sn-based materials, has attracted much attention from researchers as an important platform for heterostructure-sensing applications owing to its layered structure, appropriate mid-bandgap, high surface activity, easy surface functionalization, and large electronegativity [27]. The SnO₂ band is more positive than the SnS₂ band, resulting in the photoexcitation of electrons and their movement from the SnS₂ conduction band to SnO₂ until the equilibrium of the Fermi level is reached. This process forms n–n heterojunctions. Since the chemical and physical properties of SnO₂ and SnS₂ are very similar, they can interact well at the interface. The high electron mobility through the phases promotes the adsorption of chemical species on the material's surface, including the chemisorption of oxygen species, thereby improving the sensing properties. Along this line, some previous works have recently reported constructing SnO₂/SnS₂ heterojunctions for detecting toxic gas. For example, hollow core-shell-structured SnO₂@SnS₂ [28] and SnS₂/SnO₂ heterojunctions [29] both showed a superior response to NO₂. Meanwhile, the response value of a flexible NH₃ gas sensor based on SnO₂/SnS₂ is twice that of pure SnO₂ at room temperature [30]. Inspired by the studies above, it is proposed that the construction of SnS₂/SnO₂ heterojunctions on SnO₂ micro-nanostructures presents a promising strategy to overcome the bottleneck of insensitivity at room temperature. Nevertheless, to date, there has been a lack of research on the formaldehyde-sensing performances of SnS₂/SnO₂ composites at room temperature. Additionally, it remains a significant challenge to achieve well-defined SnS₂/SnO₂ composites with consistent micro-nanostructures. Furthermore, further investigation is needed to understand the sensing mechanism of SnS₂/SnO₂ composites, which holds more relevance in this field.

In this study, well-designed SnS₂/SnO₂ composites with hollow spherical structures were constructed for selective sensing of formaldehyde at room temperature, and they exhibit an ultra-high sensing response, good repeatability and stability, and ppb detection limit at room temperature. More interestingly, the SnS₂/SnO₂ composites have extraor-

dinary formaldehyde selectivity, demonstrating almost no response for several common interfering gases. Density functional theory (DFT) simulations showed that the SnS₂/SnO₂ composites could effectively enhance the adsorption energy toward formaldehyde, contributing to its excellent selectivity. Moreover, the n–n heterojunction formed between SnO₂ and SnS₂ boosts the potential barrier at the interface, and the unique hollow structures bring more active sites along the material's surface, thereby improving the sensing response. This work demonstrates that constructing SnS₂/SnO₂ heterojunctions on the SnO₂ hierarchical structure efficiently develops next-generation room-temperature gas sensors with an improved sensing performance.

2. Experimental

2.1. Materials and Chemicals

The chemicals used in the experiment, including tin (IV) chloride pentahydrate (SnCl₄·5H₂O), sodium hydroxide (NaOH), acetic acid (C₂H₄O₂), thiourea (CH₄N₂S), formaldehyde (HCHO), ethanol (CH₃CH₂OH), acetone (CH₃COCH₃), methanol (CH₃OH), trimethylamine (C₃H₉N), benzene (C₆H₆), and toluene (C₇H₈), were analytical-grade reagents.

2.2. Synthesis of SnO₂ Hollow Spheres

The SnO₂ hollow spheres were prepared via a facile hydrothermal route. Briefly, 1.73 g SnCl₄·5H₂O, 1.25 g NaOH, and 30 mL of deionized water were added to a glass beaker and vigorously stirred for 30 min. Then, the clarified solution was poured into a 50 mL Teflon-lined stainless-steel autoclave and reacted at 200 °C for 24 h. After natural cooling to room temperature, the precipitate was collected, washed with deionized water and ethanol for 6 cycles, and then dried overnight at 60 °C to obtain the SnO₂ hollow spheres.

2.3. Synthesis of SnS₂/SnO₂ Composites with Hollow Spherical Structures

Similarly, a series of SnS₂/SnO₂ composites with hollow spherical structures were also synthesized using a facile hydrothermal method. After introducing thiourea into the synthesis system, a portion of SnO₂ was converted into SnS₂; the detailed synthesis process can be found in the Supplementary Materials.

2.4. Synthesis of SnS₂/SnO₂ Composites with Hollow Spherical Structures

The detailed characterization of the crystal structure, morphology characteristics, elemental analysis, surface valence states, specific surface area, electrochemical testing, and electron paramagnetic resonance can be found in the Supplementary Materials.

2.5. Fabrication and Measurement of Sensors

The gas sensor was fabricated as follows. Firstly, a homogeneous slurry of either SnO₂ or SnS₂/SnO₂ was prepared by dispersing the synthesized products (40 mg) in ethanol. This slurry was then coated onto the surface of an Al₂O₃ ceramic tube (4 mm in length, 1.2 mm in external diameter, and 0.8 mm in internal diameter). At each end of the Al₂O₃ ceramic tube, there were two Au electrodes, which were connected to two Pt lead wires. After natural drying, a Ni–Cr alloy coil was inserted through the central tunnel of the ceramic tube to act as a heater and regulate the operating temperature of the gas sensor. The Pt lead wires and the Ni–Cr heating wire were soldered on a four-corner base to fabricate the gas sensor. To enhance the stability and repeatability of the fabricated gas sensor, it was aged on a TS60 desktop (Winsen Electronics Co., Ltd., Zhengzhou, China) at 200 °C for 48 h. The gas-sensing tests were carried out in a static system (Weisheng Tech Co., Ltd., Zhengzhou, China) at room temperature. This work defines the sensor's response as the resistance ratio, $S = R_a/R_g$ (R_g : resistance in testing gas, R_a : resistance in the air). The schematic diagram of the synthesis process of the SnS₂/SnO₂ composites and the fabricated gas sensor is illustrated in Figure 1.

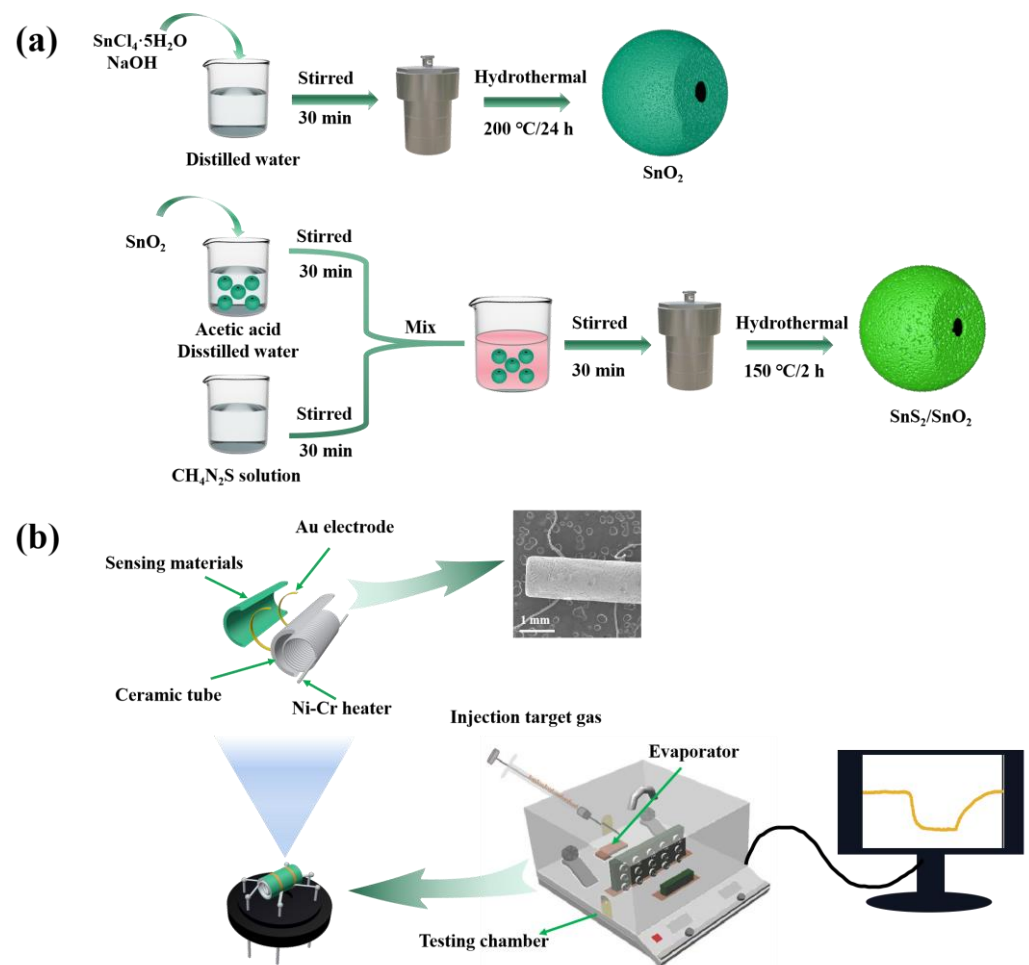


Figure 1. (a) Schematic illustration of the synthesis process of the SnS₂/SnO₂ composites. (b) Schematic illustration and corresponding SEM image of the gas sensor, and schematic illustration of measurement system.

3. Results and Discussion

3.1. Structural and Morphological Characteristics

The appearance and morphology of the SnO₂ and SnS₂/SnO₂ samples are shown in Figure 2. Obviously, pure SnO₂ is composed of numerous spherical architectures with a diameter of approximately 2~4 μm (Figure 2a), and it can be seen that the spherical architecture is hierarchically constructed by many primary particles with a size of a few dozen nanometers in the amplifying FE–SEM images (Figure 2b), whose more detailed structure can be seen clearly in a broken SnO₂ sphere. Interestingly, after the sulfurization of SnO₂ (Figure 2c–h), the sample still maintains a hollow spherical structure with almost no change in size; however, compared to the SnO₂ sample, the hollow sphere surface of SnS₂/SnO₂ becomes rough, which may be due to the formation of SnS₂ nanoparticles on the SnO₂ hollow sphere surface. The FE–SEM images exhibit porous, rough surface structures, which can absorb more gas and accelerate gas transmission, resulting in an improvement in the gas-sensing properties. According to the EDS mapping images of SnS₂/SnO₂–2 in Figure 2i–l, it can be seen that the three elements, namely, Sn, S, and O, are uniformly distributed on the surface, confirming the existence of SnS₂ and SnO₂.

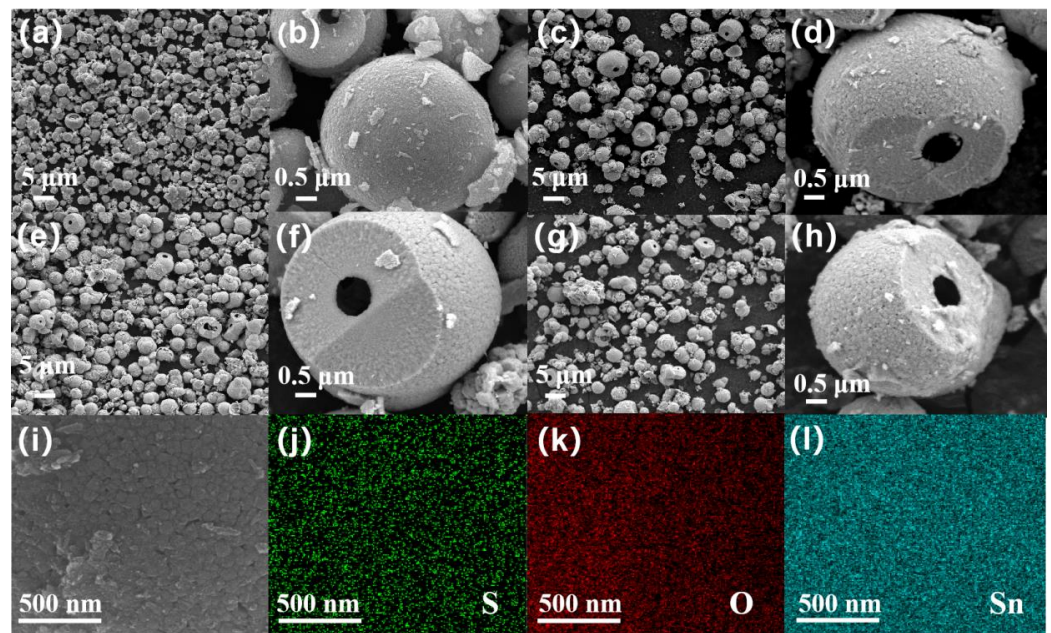


Figure 2. The FE-SEM images of (a,b) SnO_2 , (c,d) $\text{SnS}_2/\text{SnO}_2$ -1, (e,f) $\text{SnS}_2/\text{SnO}_2$ -2, and (g,h) $\text{SnS}_2/\text{SnO}_2$ -3. (i–l) EDS elemental mapping images of $\text{SnS}_2/\text{SnO}_2$ -2.

Furthermore, the crystal structures of the SnO_2 and $\text{SnS}_2/\text{SnO}_2$ samples were analyzed using XRD. As shown in Figure 3, the diffraction peaks of the SnO_2 hollow spheres at 2θ of 26.6° , 33.9° , 38.9° , 51.8° , and 54.7° correspond to the (110), (101), (111), (211), and (220) crystal planes of SnO_2 , respectively, which is in good agreement with the tetragonal SnO_2 phase (JCPDS No. 41-1445). After the sulfurization of SnO_2 , all the crystal phases belong to SnO_2 and SnS_2 , confirming the formation of $\text{SnS}_2/\text{SnO}_2$ composites. Apart from the peaks belonging to pure SnO_2 , the weak diffraction peaks at about 29.3° , 32.1° , and 50.1° are assigned to the (101), (102), and (110) planes of SnS_2 (JCPDS no. 21-1231). Additionally, no excess impurity peaks indicate the high purity of the as-synthesized samples.

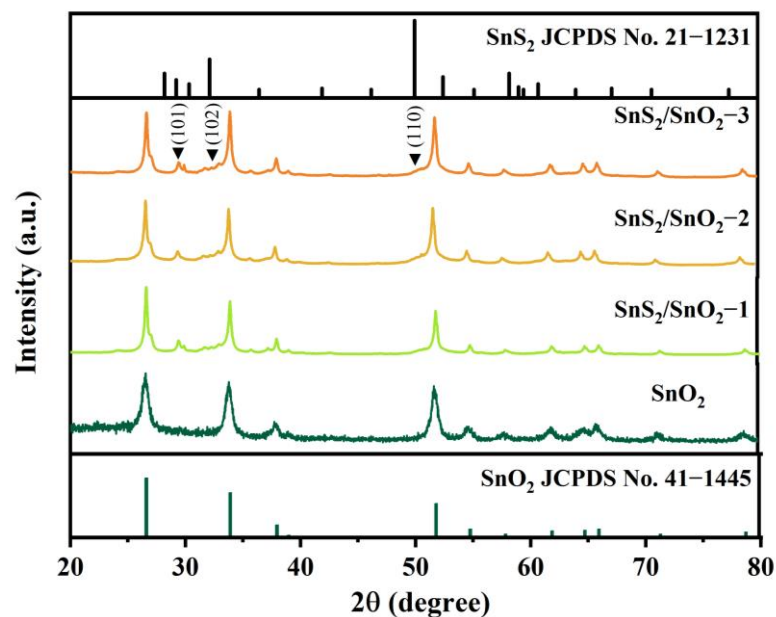


Figure 3. XRD patterns of SnO_2 and $\text{SnS}_2/\text{SnO}_2$ samples.

In order to further investigate the internal microstructure and crystal structure of the $\text{SnS}_2/\text{SnO}_2$ composites, TEM and HRTEM analyses were conducted (Figure 4), which

revealed that the material has a hollow spherical structure observed from the broken material (Figure 4a). Moreover, a loose and porous surface can be observed in Figure 4b, which is in accordance with the results of the FE-SEM analyses. Figure 4c–g illustrates well-defined lattice stripes of the SnS₂/SnO₂ composites. The crystallographic distances of 0.34, 0.18, and 0.28 nm correspond to the (110) crystallographic planes of SnO₂, and the (110) and (102) crystallographic planes of SnS₂, respectively. These values align with the dominant peaks observed in the XRD patterns. Furthermore, the lattice stripes observed between SnS₂ and SnO₂ exhibit a seamless continuity, indicating the successful formation of an n–n heterojunction.

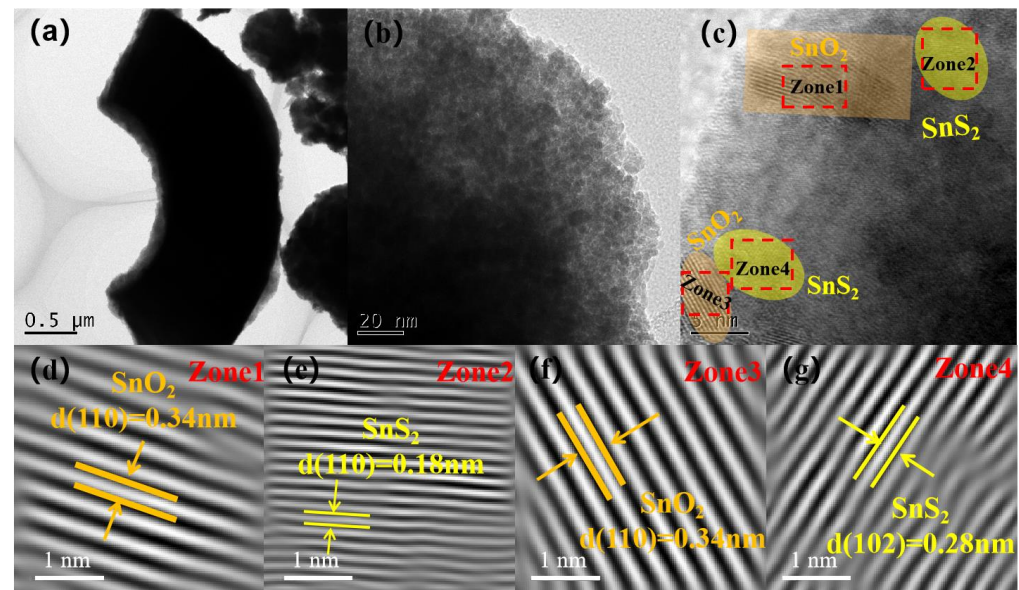


Figure 4. TEM image (a) and (b–g) corresponding HR-TEM image of SnS₂/SnO₂–2 composites.

The elemental composition and chemical state of the SnO₂ and SnS₂/SnO₂–2 composites were characterized by XPS analysis, and the pure SnO₂ comprises Sn and O (Figure 5a). In contrast, the SnS₂/SnO₂ composites contain Sn, O, and S. Notably, the signal peak of C is caused by contaminated carbon or corrected carbon. The Sn 3d spectrum of both pure SnO₂ and the SnS₂/SnO₂ composites (Figure 5b) exhibits two peaks at 486.1 and 494.5 eV (SnO₂) and 486.6 and 494.9 eV (SnS₂/SnO₂), conforming with Sn 3d_{5/2} and Sn 3d_{3/2}, respectively. This confirms the presence of Sn in the samples as a Sn⁴⁺ form [29,31]. Additionally, the Sn 3d peaks of the SnS₂/SnO₂ composites exhibit a slight shift towards a higher binding energy compared to pure SnO₂, which suggests that there is some interaction between SnO₂ and SnS₂ in the composites [32]. In Figure 5c, the O 1s asymmetric peak of pure SnO₂ can be divided into three peaks at 530.0 eV, 531.0 eV, and 531.9 eV, which are attributed to lattice oxygen (O_L), oxygen vacancies (O_V), and surface-absorbed oxygen (O_C), respectively [33]. The O 1s peaks of the SnS₂/SnO₂ composites are slightly shifted towards the high energy direction at 530.4 eV, 531.3 eV, and 532.4 eV, corresponding to O_L, O_V, and O_C, respectively. Generally, the O_V can promote gas absorption and reaction by providing abundant active sites, and O_C directly affects the chemical adsorption and ionized oxygen state on the surface of sensing materials; hence, a high ratio of O_V and O_C is favorable for achieving good gas-sensing properties [34]. Through calculation, it was found that the concentration of O_V (25.1%) and O_C (11.6%) in SnS₂/SnO₂ are higher than those of pure SnO₂ O_V (17.2%) and O_C (10.4%), indicating its good sensing performance. In addition, the S 2p spectrum can be divided into two peaks at 161.7 eV and 163.1 eV (Figure 5d), corresponding to S 2p_{3/2} and S 2p_{1/2}, respectively [35]. The results further indicate that the as-synthesized samples are SnS₂/SnO₂ composites.

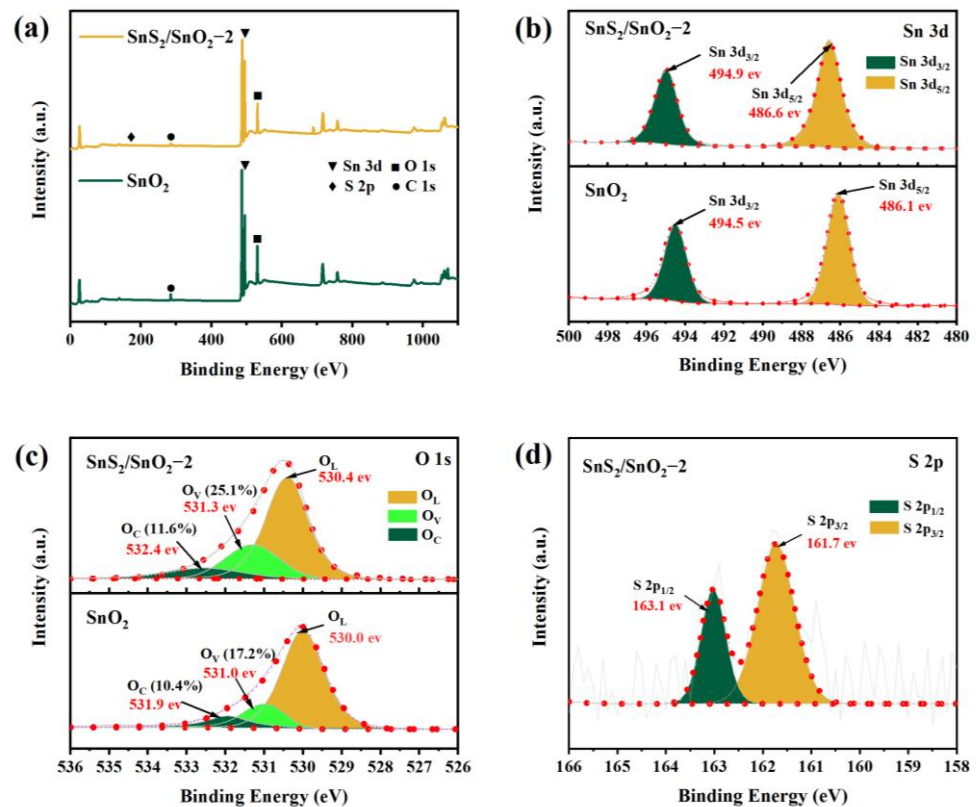


Figure 5. XPS spectra of SnO₂ and SnS₂/SnO₂-2 samples. (a) Survey spectrum, (b) Sn 3d spectrum, (c) O 1s spectrum, and (d) S 2p spectrum.

To further confirm the presence of oxygen vacancies in the samples, electron paramagnetic resonance (EPR) spectra of the SnO₂ and SnS₂/SnO₂-2 were developed, as shown in Figure 6. The EPR spectra were measured at a temperature of 25 °C using a Bruker EMXPLUS spectrometer operating at the X band with a magnetic field modulation of 100.00 kHz. The microwave power was set to 3.170 mW and the modulation amplitude was 1.000 G [36]. Both samples revealed a strong signal corresponding to $g(I) = 2.003$, suggesting the presence of oxygen vacancies. The g value was determined by a comparison with a DPPH standard [37]. In addition, the signal intensity of SnS₂/SnO₂-2 is higher than that of SnO₂, supporting the XPS results that the oxygen vacancy content increases after partial sulfurization of SnO₂ to SnS₂.

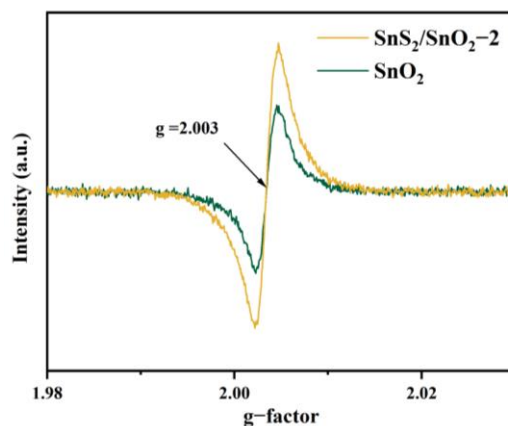


Figure 6. EPR spectra of SnO₂ and SnS₂/SnO₂-2 hollow spheres.

3.2. Gas-Sensing Properties

The formaldehyde-sensing properties of SnO₂, SnS₂, and SnS₂/SnO₂ hollow spheres were studied at room temperature. Figure 7a shows the transient resistance curve of SnO₂, SnS₂, SnS₂/SnO₂-1, SnS₂/SnO₂-2, and SnS₂/SnO₂-3 sensors to 0.1 ppm formaldehyde. Obviously, it is hard to obtain the sensing behavior of the SnO₂ and SnS₂ sensor at this low concentration. As for the SnS₂/SnO₂ sensors, an obvious response and recovery performance towards formaldehyde was observed, where the resistance decreased upon exposure to formaldehyde and recovered to its initial value after exposure to clean air, exhibiting typical n-type semiconductor characteristics. In addition, their response to formaldehyde is determined by the amount of S (Figure 7a). Notably, the SnS₂/SnO₂-2 sensor shows the highest response value of 1.93, meaning it has an excellent sensing ability for detecting trace formaldehyde in the atmosphere. Figure 7b shows the transient resistance curves and response value of five gas sensors to 10 ppm formaldehyde at room temperature, wherein the SnO₂ and SnS₂ sensor still had no response to formaldehyde at a relatively high concentration. In contrast, the SnS₂/SnO₂ sensor showed a significant increase in the response and recovery amplitudes, indicating that sulfurization functionalized SnO₂ forming SnS₂/SnO₂ heterostructures can significantly improve the sensing ability of SnO₂ hollow spheres. The selectivity of four sensors was investigated by comparing the sensing response to various reducing gases (formaldehyde, acetone, methanol, TMA, benzene, and toluene) with concentrations of 0.1 ppm and 10 ppm at room temperature (Figure 7c,d). Obviously, the SnO₂ sensor had no response to any of the test gases at low or high concentrations (0.1 or 10 ppm), suggesting its poor sensing activity at room temperature. In contrast, all the SnS₂/SnO₂ sensors responded well to formaldehyde and were not very sensitive to other interfering gases. Specifically, the SnS₂/SnO₂-2 sensor was more sensitive to formaldehyde than the other sensors, demonstrating that it is more suitable for trace formaldehyde detection, and the following sensing performance was focused on the SnS₂/SnO₂-2 sensor.

The transient resistance curve of the SnS₂/SnO₂-2 sensor to a low formaldehyde concentration (0.1–1 ppm) and high formaldehyde concentration (10–100 ppm) is shown in Figure 8a,c. The corresponding response is plotted against the formaldehyde concentration, and it is apparent that the resistance decreased rapidly and reached a certain level after some time (Figure 8b,d). In contrast, upon removing formaldehyde from the chamber, the resistance gradually recovered to its original baseline value, confirming its good reproducibility. As the formaldehyde concentration increased, the response improved significantly (0.1–1 ppm), but when the formaldehyde concentration was above 10 ppm, the magnitude of the rise in response gradually slowed down due to the high surface coverage of formaldehyde [38]. In addition, the response versus the formaldehyde concentration (0.1–1 ppm) presents a good linear relationship with a fitting slope of 8.44408 ppm⁻¹ (Figure 8b) [39]. The theoretical detection limit is calculated to be approximately 5.81 ppb based on the signal-to-noise ratio (see the Supplementary Materials for details). Such results suggest that the SnS₂/SnO₂-2 sensor in this work can potentially monitor ppb-level formaldehyde in the environment.

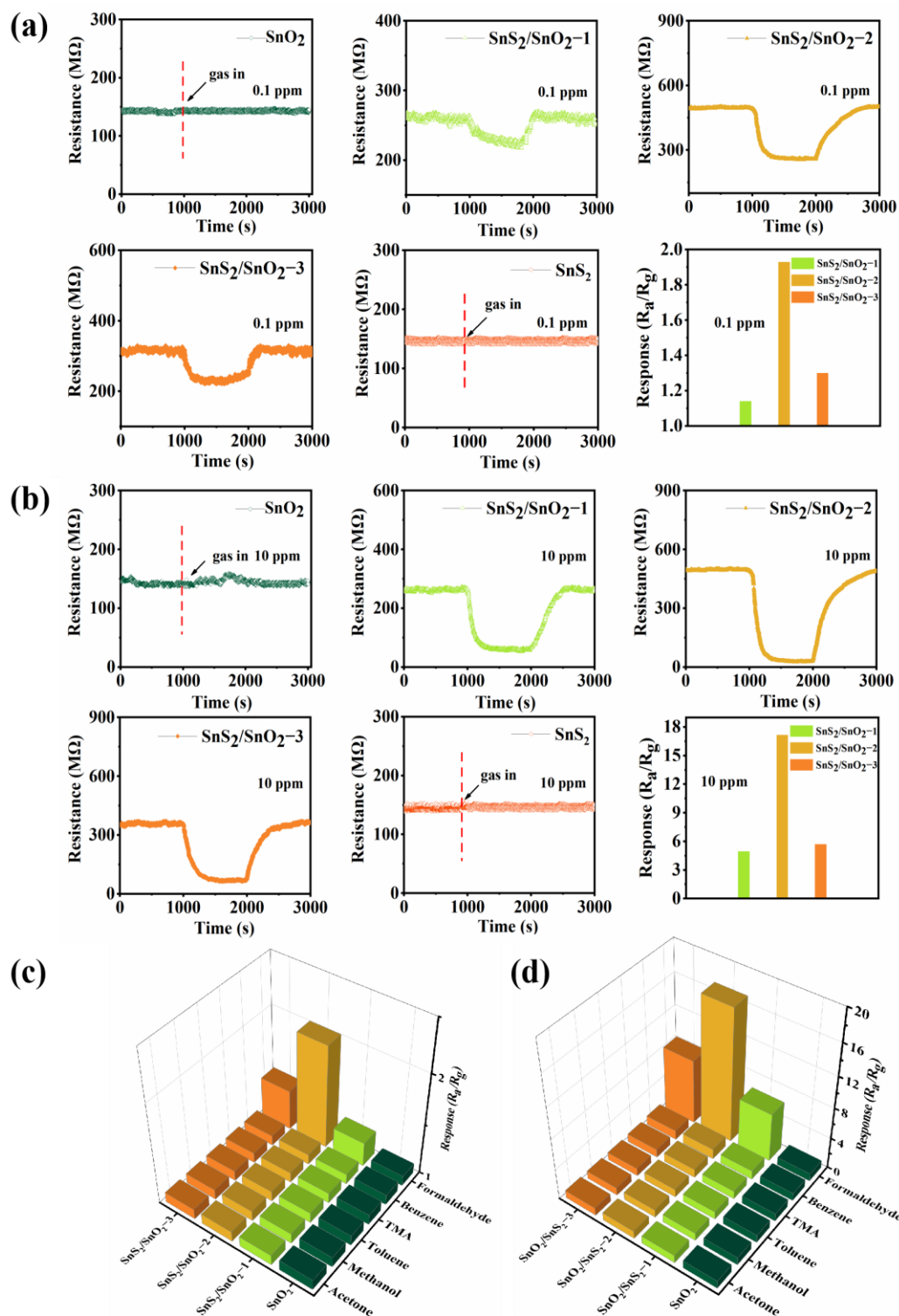


Figure 7. Gas-sensing properties of the sensors at room temperature: dynamic response recovery curve and corresponding response of SnO₂, SnS₂, and SnS₂/SnO₂ hollow spheres at room temperature to (a) 0.1 ppm formaldehyde and (b) 10 ppm formaldehyde; selectivity of SnO₂ and SnS₂/SnO₂ sensors to six different gases at room temperature at (c) 0.1 ppm and (d) 10 ppm.

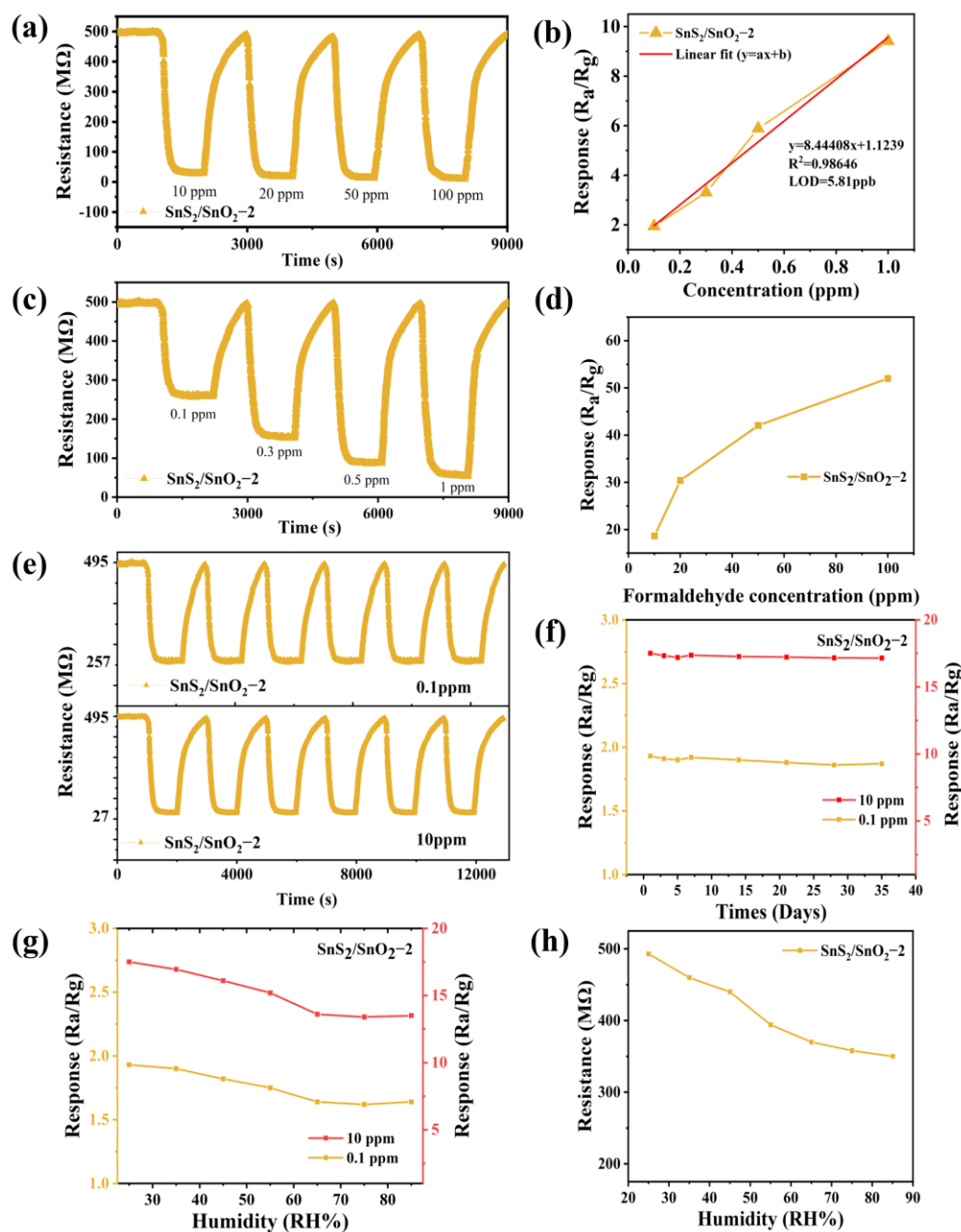


Figure 8. Gas-sensing properties of the $\text{SnS}_2/\text{SnO}_2-2$ sensor at room temperature: (a) dynamic response recovery curve and (b) correlation curve of the response with formaldehyde concentration (0.1–1 ppm); (c) dynamic response recovery curve and (d) corresponding response with formaldehyde concentration (10–100 ppm); (e) repeatability, (f) long-term stability, (g) response changes under varying humidity to formaldehyde (0.1 ppm or 10 ppm), and (h) the variation of baseline resistance versus relative humidity.

Repeatability and stability are essential parameters for practical applications. The repeatability of the $\text{SnS}_2/\text{SnO}_2-2$ sensor was investigated by exposing it to 0.1 ppm or 10 ppm formaldehyde in five cycles of response-recovery at room temperature (Figure 8e). Each cycle exhibited similar adsorption-desorption trends, and the initial resistance value did not change significantly. Additionally, the response also showed slight fluctuations in each trial, implying its good repeatability. Furthermore, the formaldehyde-sensing response of the $\text{SnS}_2/\text{SnO}_2-2$ sensor was monitored for 35 days to identify its long-term stability (Figure 8f). Interestingly, there was no significant decrease in the response over the testing period; even 35 days later, the response remained at 96.89% (0.1 ppm) and 97.94% (10 ppm),

indicating its good long-term stability. At room temperature, humidity is also an essential factor affecting the sensor's practical application. The effect of relative humidity (RH) on the formaldehyde-sensing response (0.1 ppm or 10 ppm) at room temperature was explored, and the result is shown in Figure 8g. It was found that in the range of RH from 25% to 55%, the response to 0.1 ppm or 10 ppm formaldehyde decreased slightly with increasing RH levels. In contrast, the decrease in response was relatively higher when the RH value was above 55%, which could be originated from the adsorption competition between oxygen species and water molecules on the sensor surface, hindering the redox reaction of the target gas [40]. A reduction of the baseline resistance as the RH levels increased was also observed (Figure 8h), implying the occurrence of surface reactions between water molecules and the adsorbed oxygen species [41]. In addition, Table 1 compares the results of this work and others reported in the literature for formaldehyde detection. Compared to the previously described sensing material, the SnS₂/SnO₂-2 composites offer more significant potential for a formaldehyde-sensing ability at room temperature due to their high responses and low detection limit.

Table 1. Comparison of sensing ability of gas sensors based on different sensing materials toward formaldehyde.

Materials	Temperature (°C)	Concentration (ppm)	Response (Ra/Rg)	Res./Rec. Time (s)	LOD	References
Sn ₃ O ₄ /rGO	150	100	44	4/125	1 ppm	[1]
PdPt/SnO ₂	190	1	83.7	5/7	50 ppb	[42]
In ₂ O ₃ /TiO ₂	RT	1	3.8	28/50	0.06 ppm	[43]
In ₂ O ₃ /ANS/rGO	RT	0.5	2.4	119/179	5 ppb	[44]
Ni-In ₂ O ₃ /WS ₂	RT	20	32	76/123	15 ppb	[45]
C/rh-In ₂ O ₃	120	50	330	12/355	11 ppb	[46]
MXene/Co ₃ O ₄	RT	10	9.2	0.17/0.19	0.01 ppm	[47]
Bi doped Zn ₂ SnO ₄ /SnO ₂	180	50	23.2	16/9	--	[48]
2 at% Al-doped ZnO	320	50	6.8	81/21	0.5 ppm	[49]
SnO ₂ /ZSM-5	250	10	11.67	37/115	2 ppm	[50]
SnS ₂ /SnO ₂	RT	0.1	1.93	227/424	5.81 ppb	This work

3.3. Gas-Sensing Mechanism

Generally, the sensing mechanism of SnO₂ sensors is related to the resistance modulation caused by the chemical interaction between the absorbed target gas and ionized oxygen species on the SnO₂ [51]. In this work, the SnO₂ and SnS₂/SnO₂ composites showed a typical n-type sensing feature, meaning that electrons act as the major charge carriers for sensing reactions. This is also confirmed by the Mott-Schottky analyses, and both SnO₂ and SnS₂/SnO₂-2 hollow spheres show a positive slope in the M-S plots (Figure 9a), indicating that electrons act as the leading carriers and exhibit n-type semiconductor conduction characteristics. Subsequently, the flat band potential (U_{FB}) of the composite was ascertained by calculating the intercept of the linear segment of the Mott-Schottky curve of the SnS₂/SnO₂-2 composite with the potential axis [52]. The U_{FB} of the composite is -0.43 V (standard hydrogen electrode, SHE). For the pure SnO₂ hollow spheres, electrons from the conduction band can react with the oxygen molecules in the ambient atmosphere to form oxygen anions (O₂⁻, O⁻, and O²⁻), depending on the operational temperatures. This process forms an electron depletion layer on the SnO₂ surface, thereby increasing the resistance (Ra) of the SnO₂ sensor in the air. Usually, at room temperature, the surface oxygen species were mainly O₂⁻. Upon exposure to reducing gas (formaldehyde), the ionized oxygen species could react with the formaldehyde molecules to release the trapped electrons into the SnO₂ conduction band, thereby narrowing the thickness of the electron depletion layer and reducing the resistance value of the sensor (Rg). The chemical reactions are as follows [53–55]:



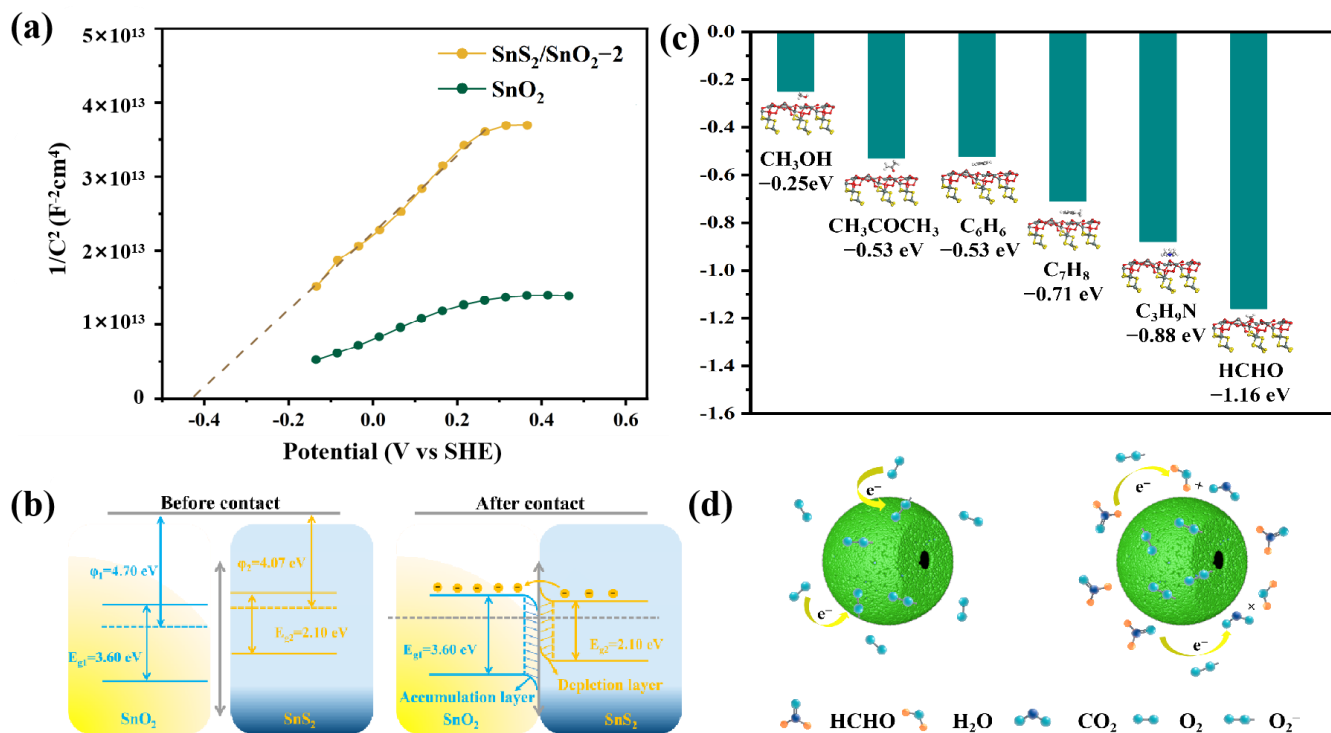
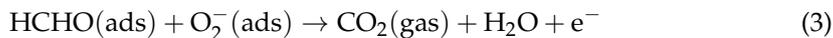


Figure 9. (a) Mott–Schottky plots of the SnO₂ and SnS₂/SnO₂–2 hollow spheres; (b) energy band structure diagram of the SnS₂/SnO₂ heterojunctions; (c) DFT-calculated adsorption energies of the SnS₂/SnO₂ heterojunction surface; (d) schematic diagram of sensing mechanism of SnS₂/SnO₂ hollow spheres in air and formaldehyde.

The reasons for the improved gas-sensing performance of the SnS₂/SnO₂ composite materials, unlike single-type SnO₂, are as follows.

- (1) The existence of an n–n heterojunction plays a crucial role in enhancing the sensing performance. The difference between the electronic work function of SnO₂ and SnS₂ makes the electrons in SnS₂ flow to SnO₂ until the Fermi level reaches equilibrium [28] when they contact each other (Figure 9b). The transfer of electrons and the significant difference in electron work functions result in band bending within the material, further causing the accumulation of electrons at the surface of SnO₂ and the depletion of electrons at the surface of SnS₂. Meanwhile, a potential barrier is generated between the heterojunction architecture. As the SnS₂/SnO₂ is exposed to the air environment, more ionized oxygen species are absorbed on the surface of the sensing materials, leading to a more significant initial resistance state immediately. When it is exposed to formaldehyde, the sensing reaction of the oxygen species with formaldehyde releases more electrons back to the conduction band. This process narrows the electron depletion layer, dramatically decreasing the sensor resistance with the reduced heterojunction potential barrier height; thus, the SnS₂/SnO₂ heterojunction configuration significantly enhances the sensor's capabilities.
- (2) The oxygen/formaldehyde adsorption capacity has an important impact on the gas-sensing performance of the materials. The XPS and EPR analyses show that the SnS₂/SnO₂ composites process more oxygen vacancies, implying their high oxygen adsorption capacity. Upon exposure to formaldehyde, more oxygen species means

more formaldehyde molecules can react, consequently leading to a high gas-sensing ability. At the same time, the enhanced adsorption ability of the SnS₂/SnO₂ composites was revealed through DFT calculations, which were performed employing the CASTEP module in Materials Studio software (see the Supporting Information and Figure S2 for details). As shown in Figure 9c, when the sensor is in contact with the tested gas molecules, the adsorption energy of formaldehyde on the (110)/(101) plane of SnS₂/SnO₂ is −1.11 eV, which is much larger than that of the other tested gases (acetone: −0.53 eV, methanol: −0.25 eV, toluene: −0.71 eV, benzene: −0.53 eV, TMA: −0.88 eV, formaldehyde: −1.16 eV). This indicates a strong interaction between formaldehyde and the SnS₂/SnO₂ surface, directly proving the improved sensing performance to formaldehyde from the energy point of view.

- (3) The unique structural merits, including the hollow and porous structure, are also essential in improving the gas-sensing performance. The hollow, mesoporous structure of the SnS₂/SnO₂ composites significantly contributes to the specific surface area (Figure 9d). The BET measurements (see the Supporting Information and Figure S1 for details) revealed that both SnO₂ and SnS₂/SnO₂ hollow spheres possess a high specific surface area, and the SnS₂/SnO₂-2 hollow spheres (92.5 m² g^{−1}) have a higher specific surface area than that of SnO₂ (87.4 m² g^{−1}). This indicates that the SnS₂/SnO₂-2 hollow spheres can provide many active sites for the adsorption of oxygen species and formaldehyde gas, booting the resistance modulation. In addition, the porous channel structure can essentially promote the penetration efficiency of air/target molecules in the sensing interaction, boosting the reaction of formaldehyde and oxygen species.

Overall, the synergistic effect of the n–n heterojunctions between SnO₂ and SnS₂, the strong oxygen/formaldehyde adsorption capacity, and the unique structural merits, including the hollow and porous structure, enhance the formaldehyde-sensing performance in the SnS₂/SnO₂ composites; however, excessive SnS₂ can decrease the sensor response, as it can hide the SnO₂ surface and become the dominant conductive path, hindering the desired sensing function. Moreover, increasing the SnS₂ content further degrades the quality of the n–n heterojunction, weakening its effect. Based on the results, the SnS₂/SnO₂-2 sensor with optimized decoration significantly improves the formaldehyde-sensing properties of the material, making it a more effective gas sensor for detecting this harmful gas.

4. Conclusions

In summary, SnS₂/SnO₂ heterostructures with hollow spherical structures were synthesized by a simple hydrothermal method for highly sensitive and selective formaldehyde detection. Benefiting from the synergistic effect of the n–n heterojunction between SnO₂ and SnS₂, strong oxygen/formaldehyde adsorption capacity, and unique structural features, including the hollow and porous structure, the SnS₂/SnO₂ sensor presents a superior formaldehyde-sensing performance at room temperature. Remarkably, the SnS₂/SnO₂-2 sensor demonstrates exceptional selectivity, detecting formaldehyde in concentrations as low as 0.1 ppm, with the highest sensing response of 1.93. Furthermore, the sensor exhibits good repeatability, long-term stability, and an outstanding theoretical detection limit. To gain further insight into the enhanced gas-sensing performance, we conducted DFT calculations, which shed light on the underlying mechanism. The excellent comprehensive gas-sensing properties enable SnS₂/SnO₂ hollow spheres to position themselves as highly selective gas-sensing platforms for the detection of trace amounts of formaldehyde. This technology is well-suited for energy-saving and portable detection systems, meeting the demands of various applications.

Supplementary Materials: The following supporting information can be downloaded at: <https://www.mdpi.com/article/10.3390/nano13172493/s1>, Figure S1: N₂ adsorption–desorption isotherms and corresponding BJH pore size distribution curves of (a) SnO₂ and (b) SnS₂/SnO₂-2 hollow spheres.

Figure S2. Optimized adsorption configurations of (a) formaldehyde, (b) ethanol, (c) methanol, (d) benzene, (e) toluene, and (f) trimethylamine on the SnO₂/SnS₂ surface.

Author Contributions: Conceptualization, Z.X.; data curation, Z.X.; formal analysis, Z.X., M.W., G.W., and Y.Z.; funding acquisition, D.M.; investigation, Z.X.; methodology, D.M., Z.X., J.Q., and Q.J.; project administration, D.M., X.S., and J.Q.; resources, G.W.; supervision, X.S., J.Q., and Q.J.; validation, D.M. and J.X.; visualization, Z.X. and Y.Z.; writing—original draft, Z.X.; writing—review and editing, D.M., J.Q., and Q.J. All authors have read and agreed to the published version of the manuscript.

Funding: This research was funded by the National Natural Science Foundation of China, grant number 61973223; the Liao Ning Revitalization Talents Program, grant number XLYC2007051; the Education Department Foundation of Jilin Province, grant number JJKH20220997KJ; the Support Plan for Innovative Talents in Colleges and Universities in Liaoning Province, grant number 2020389; the Liaoning Educational Department Foundation, grant number LJKMZ20220762; the Natural Science Foundation of Liaoning Province, grant number 2021-MS-257; and the Young and Middle-aged Scientific and Technological Innovation Talents of Shenyang Science and Technology Bureau, grant number RC200352.

Data Availability Statement: Not applicable.

Conflicts of Interest: The authors declare no conflict of interest.

References

1. Das, T.; Mojumder, S.; Chakraborty, S.; Saha, D.; Pal, M. Beneficial effect of Sn doping on bismuth ferrite nanoparticle-based sensor for enhanced and highly selective detection of trace formaldehyde. *Appl. Surf. Sci.* **2022**, *602*, 154340. [CrossRef]
2. Wang, D.; Pu, X.X.; Yu, X.; Bao, L.P.; Cheng, Y.; Xu, J.C.; Han, S.C.; Ma, Q.X.; Wang, X.Y. Controlled preparation and gas sensitive properties of two-dimensional and cubic structure ZnSnO₃. *J. Colloid Interface Sci.* **2022**, *608*, 1074–1085. [CrossRef]
3. Rong, Q.; Li, Y.; Hao, S.Q.; Cai, S.T.; Wolverson, C.; Dravid, V.P.; Zhai, T.Y.; Liu, Q.J. Raspberry-like mesoporous Co-doped TiO₂ nanospheres for a high-performance formaldehyde gas sensor. *J. Mater. Chem. A* **2021**, *9*, 6529–6537. [CrossRef]
4. Yu, H.M.; Li, J.Z.; Luo, W.B.; Li, Z.Y.; Tian, Y.W.; Yang, Z.D.; Gao, X.W.; Liu, H. Hetero-structure La₂O₃-modified SnO₂-Sn₃O₄ from tin anode slime for highly sensitive and ppb-Level formaldehyde detection. *Appl. Surf. Sci.* **2020**, *513*, 145825. [CrossRef]
5. Xi, H.T.; Chen, X.G.; Cao, Y.; Xu, J.J.; Ye, C.Z.; Deng, D.W.; Zhang, J.S.; Huang, G.H. Electrochemical determination of formaldehyde via reduced AuNPs@PPy composites modified electrode. *Microchem. J.* **2020**, *156*, 104846. [CrossRef]
6. Melo Cardozo, I.M.; Sousa, E.T.; da Rocha, G.O.; Pereira dos Anjos, J.; de Andrade, J.B. Determination of free- and bound-carbonyl compounds in airborne particles by ultra-fast liquid chromatography coupled to mass spectrometry. *Talanta* **2020**, *217*, 121033. [CrossRef]
7. Xu, L.; Ge, M.Y.; Zhang, F.; Huang, H.J.; Sun, Y.; He, D.N. Nanostructured of SnO₂/NiO composite as a highly selective formaldehyde gas sensor. *J. Mater. Res.* **2020**, *35*, 3079–3090. [CrossRef]
8. Sun, Y.J.; Yang, H.Y.; Zhao, Z.T.; Suematsu, K.; Li, P.W.; Yu, Z.C.; Zhang, W.D.; Hu, J. Fabrication of ZnO quantum dots@SnO₂ hollow nanospheres hybrid hierarchical structures for effectively detecting formaldehyde. *Sens. Actuators B* **2020**, *318*, 128222. [CrossRef]
9. Krishna, K.G.; Parne, S.; Pothukanuri, N.; Kathirvelu, V.; Gandi, S.; Joshi, D. Nanostructured metal oxide semiconductor-based gas sensors: A comprehensive review. *Sens. Actuators A* **2022**, *341*, 113578. [CrossRef]
10. Pasupuleti, K.S.; Reddeppa, M.; Chougule, S.S.; Bak, N.-H.; Nam, D.-J.; Jung, N.; Cho, H.D.; Kim, S.-G.; Kim, M.-D. High performance langasite based SAW NO₂ gas sensor using 2D g-C₃N₄@TiO₂ hybrid nanocomposite. *J. Hazard. Mater.* **2022**, *427*, 128174. [CrossRef]
11. Huang, J.Y.; Liang, H.; Ye, J.X.; Jiang, D.T.; Sun, Y.L.; Li, X.J.; Geng, Y.F.; Wang, J.Q.; Qian, Z.F.; Du, Y. Ultrasensitive formaldehyde gas sensor based on Au-loaded ZnO nanorod arrays at low temperature. *Sens. Actuators B* **2021**, *346*, 130568. [CrossRef]
12. Kang, Z.J.; Zhang, D.Z.; Li, T.T.; Liu, X.H.; Song, X.S. Polydopamine-modified SnO₂ nanofiber composite coated QCM gas sensor for high-performance formaldehyde sensing. *Sens. Actuators B* **2021**, *345*, 130299. [CrossRef]
13. Zhang, D.; Wang, T.T.; Huo, L.H.; Gao, S.; Li, B.S.; Guo, C.Y.; Yu, H.X.; Major, Z.; Zhang, X.F.; Cheng, X.L.; et al. Small size porous NiO/NiFe₂O₄ nanocubes derived from Ni-Fe bimetallic metal-organic frameworks for fast volatile organic compounds detection. *Appl. Surf. Sci.* **2023**, *623*, 157075. [CrossRef]
14. Im, D.; Kim, D.; Jeong, D.; Park, W.I.; Chun, M.; Park, J.-S.; Kim, H.; Jung, H. Improved formaldehyde gas sensing properties of well-controlled Au nanoparticle-decorated In₂O₃ nanofibers integrated on low power MEMS platform. *J. Mater. Sci. Technol.* **2020**, *38*, 56–63. [CrossRef]
15. Lu, Z.C.; Ma, Z.R.; Song, P.; Wang, Q. Facile synthesis of CuO nanoribbons/rGO nanocomposites for high-performance formaldehyde gas sensor at low temperature. *J. Mater. Sci. Mater. Electron.* **2021**, *32*, 19297–19308. [CrossRef]
16. Devabharathi, N.; Umarji, A.M.; Dasgupta, S. Fully Inkjet-Printed Mesoporous SnO₂-Based Ultrasensitive Gas Sensors for Trace Amount NO₂ Detection. *ACS Appl. Mater. Interfaces* **2020**, *12*, 57207–57217. [CrossRef]

17. Das, S.; Jayaraman, V. SnO₂: A comprehensive review on structures and gas sensors. *Prog. Mater. Sci.* **2014**, *66*, 112–255. [[CrossRef](#)]
18. Meng, F.L.; Ji, H.Y.; Yuan, Z.Y.; Chen, Y.R.; Zhang, H.; Qin, W.B.; Gao, H.L. Dynamic Measurement and Recognition Methods of SnO₂ Sensor to VOCs Under Zigzag-Rectangular Wave Temperature Modulation. *IEEE Sens. J.* **2021**, *21*, 10915–10922. [[CrossRef](#)]
19. Meng, X.; Bi, M.; Xiao, Q.; Gao, W. Ultrasensitive gas sensor based on Pd/SnS₂/SnO₂ nanocomposites for rapid detection of H₂. *Sens. Actuators B* **2022**, *359*, 131612. [[CrossRef](#)]
20. Manikandan, D.; Murugan, R. Genesis and tuning of ferromagnetism in SnO₂ semiconductor nanostructures: Comprehensive review on size, morphology, magnetic properties and DFT investigations. *Prog. Mater. Sci.* **2022**, *130*, 100970. [[CrossRef](#)]
21. Yuan, Z.Y.; Zuo, K.Y.; Meng, F.L.; Ma, Z.W.; Xu, W.X.; Dong, H. Microscale analysis and gas sensing characteristics based on SnO₂ hollow spheres. *Microelectron. Eng.* **2020**, *231*, 111372. [[CrossRef](#)]
22. Yu, H.; Zhang, Y.; Dong, L.H.; Wang, J.X. Fabricating pod-like SnO₂ hierarchical micro-nanostructures for enhanced acetone gas detection. *Mater. Sci. Semicond. Process.* **2021**, *121*, 105451. [[CrossRef](#)]
23. Pandit, N.A.; Ahmad, T. Tin Oxide Based Hybrid Nanostructures for Efficient Gas Sensing. *Molecules* **2022**, *27*, 7038. [[CrossRef](#)] [[PubMed](#)]
24. Lu, Z.S.; Meng, S.J.; Ma, Z.Y.; Yang, M.X.; Ma, D.W.; Yang, Z.X.; Talib, S.H. Electronic and catalytic properties of Ti single atoms@SnO₂ and its implications on sensing mechanism for CO. *Appl. Surf. Sci.* **2022**, *594*, 153500. [[CrossRef](#)]
25. Nascimento, E.P.; Firmino, H.C.T.; Neves, G.A.; Menezes, R.R. A review of recent developments in tin dioxide nanostructured materials for gas sensors. *Ceram. Int.* **2022**, *48*, 7405–7440. [[CrossRef](#)]
26. Chen, Z.L.; Wang, D.; Wang, X.Y.; Yang, J.H. Enhanced formaldehyde sensitivity of two-dimensional mesoporous SnO₂ by nitrogen-doped graphene quantum dots. *Rare Met.* **2021**, *40*, 1561–1570. [[CrossRef](#)]
27. Li, Y.X.; Leonardi, S.G.; Bonavita, A.; Neri, G.; Wlodarski, W. Two-Dimensional (2D) SnS₂-based Oxygen Sensor. *Procedia Eng.* **2016**, *168*, 1102–1105. [[CrossRef](#)]
28. Liu, D.; Tang, Z.L.; Zhang, Z.T. Visible light assisted room-temperature NO₂ gas sensor based on hollow SnO₂@SnS₂ nanostructures. *Sens. Actuators B* **2020**, *324*, 128754. [[CrossRef](#)]
29. Gu, D.; Li, X.G.; Zhao, Y.Y.; Wang, J. Enhanced NO₂ sensing of SnO₂/SnS₂ heterojunction based sensor. *Sens. Actuators B* **2017**, *244*, 67–76. [[CrossRef](#)]
30. Bai, J.Z.; Shen, Y.b.; Zhao, S.K.; Li, A.; Kang, Z.k.; Cui, B.Y.; Wei, D.Z.; Yuan, Z.Y.; Meng, F.L. Room-Temperature NH₃ Sensor Based on SnO₂ Quantum Dots Functionalized SnS₂ Nanosheets. *Adv. Mater. Technol.* **2023**, *8*, 2201671. [[CrossRef](#)]
31. Kou, X.Y.; Meng, F.Q.; Chen, K.; Wang, T.S.; Sun, P.; Liu, F.M.; Yan, X.; Sun, Y.F.; Liu, F.M.; Shimano, K.; et al. High-performance acetone gas sensor based on Ru-doped SnO₂ nanofibers. *Sens. Actuators B* **2020**, *320*, 128292. [[CrossRef](#)]
32. Zhao, W.; He, M.; Chen, F.; Jin, X.; Duan, H.; Long, M.; Wu, Z.; Cao, B.; Yu, Y. One-pot synthesis of flower-like SnS₂/SnO₂ heterojunction with enhanced visible light photocatalytic performance. *Opt. Mater.* **2022**, *123*, 111934. [[CrossRef](#)]
33. Wang, Z.J.; Wang, F.; Hermawan, A.; Asakura, Y.; Hasegawa, T.; Kumagai, H.; Kato, H.; Kakihana, M.; Zhu, J.F.; Yin, S. SnO-SnO₂ modified two-dimensional MXene Ti₃C₂T_x for acetone gas sensor working at room temperature. *J. Mater. Sci. Technol.* **2021**, *73*, 128–138. [[CrossRef](#)]
34. Meng, X.; Bi, M.; Gao, W. Shape and composition effects of PdPt bimetallic nanocrystals on hydrogen sensing properties of SnO₂ based sensors. *Sens. Actuators B* **2023**, *390*, 133976. [[CrossRef](#)]
35. Yang, Z.; Su, C.; Wang, S.T.; Han, Y.T.; Chen, X.W.; Xu, S.S.; Zhou, Z.H.; Hu, N.T.; Su, Y.J.; Zeng, M. Highly sensitive NO₂ gas sensors based on hexagonal SnS₂ nanoplates operating at room temperature. *Nanotechnology* **2020**, *31*, 075501. [[CrossRef](#)]
36. Morazzoni, F.; Canevali, C.; Chiodini, N.; Mari, C.; Ruffo, R.; Scotti, R.; Armelao, L.; Tondello, E.; Depero, L.; Bontempi, E. Surface reactivity of nanostructured tin oxide and Pt-doped tin oxide as studied by EPR and XPS spectroscopies. *Mater. Sci. Eng. C* **2001**, *15*, 167–169. [[CrossRef](#)]
37. Yordanov, N.D.; Christova, A. DPPH as a Primary Standard for Quantitative EPR Spectrometry. *Appl. Magn. Reson.* **1994**, *6*, 341–345. [[CrossRef](#)]
38. Gao, L.P.; Fu, H.; Zhu, J.J.; Wang, J.H.; Chen, Y.P.; Liu, H.J. Synthesis of SnO₂ nanoparticles for formaldehyde detection with high sensitivity and good selectivity. *J. Mater. Res.* **2020**, *35*, 2208–2217. [[CrossRef](#)]
39. Xian, J.B.; Li, J.; Wang, W.J.; Zhu, J.Y.; Li, P.Z.; Leung, C.M.; Zeng, M.; Lu, X.B.; Gao, X.S.; Liu, J.M. Enhanced specific surface area of ZIF-8 derived ZnO induced by sulfuric acid modification for high-performance acetone gas sensor. *Appl. Surf. Sci.* **2023**, *614*, 156175. [[CrossRef](#)]
40. Lou, C.M.; Huang, Q.X.; Li, Z.S.; Lei, G.L.; Liu, X.H.; Zhang, J. Fe₂O₃-sensitized SnO₂ nanosheets via atomic layer deposition for sensitive formaldehyde detection. *Sens. Actuators B* **2021**, *345*, 130429. [[CrossRef](#)]
41. Liu, Y.; Li, X.; Li, X.; Shao, C.; Han, C.; Xin, J.; Lu, D.; Niu, L.; Tang, Y.; Liu, Y. Highly permeable WO₃/CuWO₄ heterostructure with 3D hierarchical porous structure for high-sensitive room-temperature visible-light driven gas sensor. *Sens. Actuators B* **2022**, *365*, 131926. [[CrossRef](#)]
42. Cai, H.J.; Luo, N.; Hu, Q.M.; Xue, Z.G.; Wang, X.H.; Xu, J.Q. Multishell SnO₂ Hollow Microspheres Loaded with Bimetal PdPt Nanoparticles for Ultrasensitive and Rapid Formaldehyde MEMS Sensors. *ACS Sens.* **2022**, *7*, 1484–1494. [[CrossRef](#)] [[PubMed](#)]
43. Zhang, S.; Sun, S.P.; Huang, B.Y.; Wang, N.; Li, X.G. UV-Enhanced Formaldehyde Sensor Using Hollow In₂O₃@TiO₂ Double-Layer Nanospheres at Room Temperature. *ACS Appl. Mater. Interfaces* **2023**, *15*, 4329–4342. [[CrossRef](#)]

44. Guo, L.P.; Liang, H.P.; Hu, H.Y.; Shi, S.B.; Wang, C.X.; Lv, S.T.; Yang, H.H.; Li, H.; de Rooij, N.F.; Lee, Y.-K.; et al. Large-Area and Visible-Light-Driven Heterojunctions of In₂O₃/Graphene Built for ppb-Level Formaldehyde Detection at Room Temperature. *ACS Appl. Mater. Interfaces* **2023**, *15*, 18205–18216. [[CrossRef](#)]
45. Zhang, D.Z.; Cao, Y.H.; Yang, Z.M.; Wu, J.F. Nanoheterostructure Construction and DFT Study of Ni-Doped In₂O₃ Nanocubes/WS₂ Hexagon Nanosheets for Formaldehyde Sensing at Room Temperature. *ACS Appl. Mater. Interfaces* **2020**, *12*, 11979–11989. [[CrossRef](#)] [[PubMed](#)]
46. Qin, C.; Zhang, Y.J.; Wang, Y.; Zhang, Y.; Cao, J.L. Nanoporous Mixed-Phase In₂O₃ Nanoparticle Homojunctions for Formaldehyde Sensing. *ACS Appl. Nano Mater.* **2023**, *6*, 5635–5644. [[CrossRef](#)]
47. Zhang, D.Z.; Mi, Q.; Wang, D.Y.; Li, T.T. MXene/Co₃O₄ composite based formaldehyde sensor driven by ZnO/MXene nanowire arrays piezoelectric nanogenerator. *Sens. Actuators B* **2021**, *339*, 129923. [[CrossRef](#)]
48. Zhang, R.; Ma, S.Y.; Zhang, J.L.; Wang, B.J.; Pei, S.T. Enhanced formaldehyde gas sensing performance based on Bi doped Zn₂SnO₄/SnO₂ porous nanospheres. *J. Alloys Compd.* **2020**, *828*, 154408. [[CrossRef](#)]
49. Khojier, K. Preparation and investigation of Al-doped ZnO thin films as a formaldehyde sensor with extremely low detection limit and considering the effect of RH. *Mater. Sci. Semicond. Process.* **2021**, *121*, 105283. [[CrossRef](#)]
50. Sun, Y.H.; Wang, J.; Du, H.Y.; Li, X.G.; Wang, C.; Hou, T.Y. Formaldehyde gas sensors based on SnO₂/ZSM-5 zeolite composite nanofibers. *J. Alloys Compd.* **2021**, *868*, 159140. [[CrossRef](#)]
51. Han, Z.J.; Qi, Y.; Yang, Z.Y.; Han, H.C.; Jiang, Y.Y.; Du, W.J.; Zhang, X.; Zhang, J.Z.; Dai, Z.F.; Wu, L.L.; et al. Recent advances and perspectives on constructing metal oxide semiconductor gas sensing materials for efficient formaldehyde detection. *J. Mater. Chem. C* **2020**, *8*, 13169–13188. [[CrossRef](#)]
52. Hankin, A.; Bedoya-Lora, F.E.; Alexander, J.C.; Regoutz, A.; Kelsall, G.H. Flat band potential determination: Avoiding the pitfalls. *J. Mater. Chem. A* **2019**, *7*, 26162–26176. [[CrossRef](#)]
53. Pasupuleti, K.S.; Chougule, S.S.; Vidyasagar, D.; Bak, N.-H.; Jung, N.; Kim, Y.-H.; Lee, J.-H.; Kim, S.-G.; Kim, M.-D. UV light driven high-performance room temperature surface acoustic wave NH₃ gas sensor using sulfur-doped g-C₃N₄ quantum dots. *Nano Res.* **2023**, *16*, 7682–7695. [[CrossRef](#)]
54. Shaalan, N.M.; Hamad, D. Low-temperature hydrogen sensor based on sputtered tin dioxide nanostructures through slow deposition rate. *Appl. Surf. Sci.* **2022**, *598*, 153857. [[CrossRef](#)]
55. Liu, M.; Sun, R.Y.; Sima, Z.H.; Song, P.; Ding, Y.L.; Wang, Q. Au-decorated In₂O₃ nanospheres/exfoliated Ti₃C₂T_x MXene nanosheets for highly sensitive formaldehyde gas sensing at room temperature. *Appl. Surf. Sci.* **2022**, *605*, 154839. [[CrossRef](#)]

Disclaimer/Publisher's Note: The statements, opinions and data contained in all publications are solely those of the individual author(s) and contributor(s) and not of MDPI and/or the editor(s). MDPI and/or the editor(s) disclaim responsibility for any injury to people or property resulting from any ideas, methods, instructions or products referred to in the content.